



Published in final edited form as:

Cardiovasc Pathol. 2016 ; 25(2): 127–140. doi:10.1016/j.carpath.2015.09.008.

Fenofibrate unexpectedly induces cardiac hypertrophy in mice lacking MuRF1

Traci L. Parry^{#a}, Gopal Desai^{#b}, Jonathan C. Schisler^{a,c}, Luge Li^d, Megan T. Quintana^e, Natalie Stanley^f, Pamela Lockyer^d, Cam Patterson^{a,g}, and Monte S. Willis^{a,c,d,*}

^a McAllister Heart Institute, University of North Carolina, Chapel Hill, NC, USA

^b Department of Biology, University of North Carolina, Chapel Hill, NC, USA

^c Department of Pharmacology, University of North Carolina, Chapel Hill, NC, USA

^d Department of Pathology & Laboratory Medicine, University of North Carolina, Chapel Hill, NC, USA

^e Department of Surgery, University of North Carolina, Chapel Hill, NC, USA

^f Department of Bioinformatics and Computational Biology, University of North Carolina, Chapel Hill, NC, USA

^g Presbyterian Hospital/Weill-Cornell Medical Center, New York, NY, USA

[#] These authors contributed equally to this work.

Abstract

The muscle-specific ubiquitin ligase muscle ring finger-1 (MuRF1) is critical in regulating both pathological and physiological cardiac hypertrophy in vivo. Previous work from our group has identified MuRF1's ability to inhibit serum response factor and insulin-like growth factor-1 signaling pathways (via targeted inhibition of cJun as underlying mechanisms). More recently, we have identified that MuRF1 inhibits fatty acid metabolism by targeting peroxisome proliferator-activated receptor alpha (PPAR α) for nuclear export via mono-ubiquitination. Since MuRF1 $-/-$ mice have an estimated fivefold increase in PPAR α activity, we sought to determine how challenge with the PPAR α agonist fenofibrate, a PPAR α ligand, would affect the heart physiologically. In as little as 3 weeks, feeding with fenofibrate/chow (0.05% wt/wt) induced unexpected pathological cardiac hypertrophy not present in age-matched sibling wild-type (MuRF1 $+/+$) mice, identified by echocardiography, cardiomyocyte cross-sectional area, and increased beta-myosin heavy chain, brain natriuretic peptide, and skeletal muscle α -actin mRNA. In addition to pathological hypertrophy, MuRF1 $-/-$ mice had an unexpected differential expression in genes associated with the pleiotropic effects of fenofibrate involved in the extracellular matrix, protease inhibition, hemostasis, and the sarcomere. At both 3 and 8 weeks of fenofibrate treatment, the differentially expressed MuRF1 $-/-$ genes most commonly had

* Corresponding author at: McAllister Heart Institute, Department of Pathology & Laboratory Medicine, University of North Carolina, 111 Mason Farm Road, MBRB 2340B, Chapel Hill, NC 27599, USA. Tel.: +1 919 843 1938; fax: +1 919 843 4585. monte_willis@med.unc.edu (M.S. Willis).

Disclosure statement: The authors have nothing to disclose.

Supplementary data to this article can be found online at <http://dx.doi.org/10.1016/j.carpath.2015.09.008>.

SREBP-1 and E2F1/E2F promoter regions by TRANSFAC analysis (54 and 50 genes, respectively, of the 111 of the genes >4 and <-4 log fold change; $P .0004$). These studies identify MuRF1's unexpected regulation of fenofibrate's pleiotropic effects and bridges, for the first time, MuRF1's regulation of PPAR α , cardiac hypertrophy, and hemostasis.

Keywords

MuRF1; Ubiquitin ligase; Myocyte; PPAR α ; Fenofibrate; Cardiac hypertrophy; Mitochondria

1. Introduction

The muscle-specific ubiquitin ligase muscle ring finger-1 (MuRF1) plays a critical role in the regulation of both pathological and physiological cardiac hypertrophy in vivo. Mice globally lacking the striated muscle-specific MuRF1 (MuRF1 $-/-$) exhibit an exaggerated physiological hypertrophy in response to exercise and an exaggerated pathological hypertrophy in response to pressure overload. This is attributed to MuRF1's ability to inhibit serum response factor (SRF) and insulin-like growth factor-1 (IGF-1) signaling pathways, in part, through its targeted inhibition of cJun) [1–3]. MuRF1 also has a more direct role in regulating cardiac muscle mass by targeting proteasome dependent degradation of sarcomere proteins [4–6]. MuRF1 interacts directly with cardiac troponin I, cardiac myosin binding protein-c (cMyBP-c), and myosin heavy chain, to direct their subsequent poly-ubiquitination and proteasome-dependent degradation [4,6,7]. This regulation of sarcomere degradation explains why MuRF1 $-/-$ mice have resistance to cardiac atrophy and a limited ability to regress upon unloading after the induction of pressure overload-induced cardiac hypertrophy [8]. By regulating both the indirect signaling processes that activate cardiac hypertrophy and directly targeting sarcomere proteins for degradation, MuRF1 regulates the heart's response to external stress that lead to disease.

Increasing cardiomyocyte MuRF1 inhibits fatty acid (FA) oxidation, which has been found to be mediated, in part, by MuRF1's inhibition of the FA metabolism [9]. Increasing MuRF1 inhibits peroxisome proliferator-activated receptor alpha (PPAR α) through mono-ubiquitination, which targets the nuclear export of PPAR α resulting in activity inhibition [9]. Conversely, MuRF1 $-/-$ hearts have a 500% increase in PPAR α activity, while demonstrating no significant differences in cardiac PPAR δ/β and PPAR γ activities in vivo [9]. Enhanced PPAR α activity has been attributed to the pathogenesis of diabetic heart disease, where excess dietary fat acts as a ligand to drive FA oxidation, lipid accumulation, reduced glucose utilization, and a characteristic cardiomyopathy, clinically [10]. In mice with cardiomyocyte overexpression of PPAR α , this diabetic cardiomyopathy is recapitulated, demonstrating its potential role in disease [10].

Since MuRF1 $-/-$ mice exhibit a fivefold increase in PPAR α activity, we sought to determine how challenge with fenofibrate, a PPAR α ligand, would affect the heart physiologically. In as little as 3 weeks, fenofibrate treatment induced an unexpected cardiac phenotype in MuRF1 $-/-$, but not age-matched sibling wild-type (MuRF1 $+/+$) mice. Moreover, MuRF1's regulation of fenofibrate's pleiotropic effects was identified for the first

time, connecting MuRF1's regulation of PPAR α , cardiac hypertrophy, and hemostasis for the first time.

2. Materials and methods

2.1. Animals

Twelve- to 16-week-old MuRF1 $^{-/-}$ mice [2] and age-matched MuRF1 $+/+$ controls ($n=21$; 50% male/50% female) underwent conscious echocardiography using a Vevo 770 ultrasound biomicroscopy system (VisualSonics, Inc., Toronto, Canada) as previously described [8,11,12]. Animal use was approved by the Institutional Animal Care and Use Committee at the University of North Carolina at Chapel Hill.

2.2. Fenofibrate feeding protocols

Mice were randomized to receive either standard mouse chow ($n=10$; Prolab RMH 3000; Purina LabDiet, Oxford, NC, USA) or standard mouse chow containing fenofibrate ($n=11$; 0.05% wt/wt, F6020; Sigma, St. Louis, MO, USA). Standard mouse chow and fenofibrate were sent to TestDiet (St. Louis, MO, USA) and Granville Milling (Creedmoor, NC, USA) milled the experimental fenofibrate chow. Mouse chow (fenofibrate and standard sham chow) were administered ad libitum starting on day 1 of the protocol and commencing at the end of the 3- or 8-week protocol.

2.3. Morphological analysis of the heart by histology and transmission electron microscopy (TEM)

Cardiac tissue was fixed via perfusion for use in histological analysis, as described previously [2,3]. Fixed heart tissues were paraffin embedded, sectioned, and stained with H&E or Masson's trichrome staining. Imaging of stained sections was obtained using Aperio Scanscope and Aperio Imagescope software (version 10.0.36.1805, Aperio Technologies, Inc., Vista, CA). Heart apices were fixed in preparation for transmission electron microscopy (TEM), as described previously [3], or stained with *Triticum vulgaris* lectin TRITC conjugate as previously described [2]. Myocyte area was determined using NIH ImageJ (version 1.38X) based on photomicrographs of a standard graticule ruler. Fibrosis was determined using the Aperio Imagescope's Positive Pixel Count Algorithm to analyze Masson's trichrome-stained four-chamber sections ($n=3$ /mouse), hue value=0.66 (blue), and hue width=0.1 (detection threshold above background white). The pen tool was used to isolate tissue sections to analyze, and the % fibrosis was expressed as the weighted average % of the n positive (collagen blue)/ n total (tissue, defined by the nonwhite area).

2.4. RNA isolation from cardiac tissue

Cardiac tissues were homogenized using a TissueLyser LT (Cat. #69980; Qiagen N.V., Venlo, the Netherlands) according to the manufacturer's protocols. Approximately 20–40 mg of apical ventricle was homogenized in 1 ml of Trizol (Cat. #15596-026; Life Technologies, Inc., Carlsbad, CA, USA) using a 5-mm stainless steel bead (Cat. #69989; Qiagen, N.V.). Chloroform (200 μ l) was added and centrifuged at 12,000g (15 min at 4°C), isopropanol (0.5 ml) was added to the aqueous phase and centrifuged at 12,000g (10 min at 4°C), and the resulting RNA pellet was washed with 1 ml of 75% ethanol, dried, and

resuspended in RNase-free water. RNA concentration was then determined by UV spectroscopy (absorbance of 260–280 nm).

2.5. Real-time polymerase chain reaction and statistical analysis

RNA (500 ng) was reverse-transcribed using iScript reverse transcription supermix (Cat. #170-8841; Bio-Rad, Laboratories, Inc., Hercules, CA, USA). Gene expression assays were performed using Taqman Gene Expression Assays (Life Technologies) and Universal Taqman Master mix (Life Technologies, Cat. #4304437). Cardiac hypertrophy fetal gene expression was monitored using probes for beta-myosin heavy chain (β -MHC; Mm00600555_m1), skeletal muscle α -actin (Mm00808218_g1), and brain natriuretic peptide (BNP; Mm00435304_g1) mRNA. MuRF1's regulation of PPAR-associated genes was monitored using probes for *CD36* (Mm00432403_m1), *CPT-1* (Mm00487200_m1), *PGC-1* (Mm00447183_m1), *PDK4* (Mm00443325_m1), *FATP1* (Mm00449811_m1), *PRKAA2* (Mm01264791_g1), *PPAR α* (Mm00440939_m1), *PPAR β* (Mm01305434_m1), *Acox1* (Mm00443579_m1), *FABP3* (Mm00445880_1), *FABP4* (mm0232494_m1), *LPL* (Mm00434770_m1), and reference 18S (Hs99999901_s1). Mitochondrial number was quantified by quantitative polymerase chain reaction (qPCR), and DNA was isolated from 50 μ l whole-heart homogenates using the DNAeasy Blood and Tissue Kit (Qiagen; Cat. #69506). Isolated DNA and oligomer primers for mitochondrial cytochrome *c* oxidase subunit 1 (CO1; aka mt-CO1), cytochrome *b* (Cyt-b; aka mt-Cyb), and NADH dehydrogenase 1 (ND1; aka mt-nd1) DNA normalized to nuclear H19 (imprinted maternally expressed transcript, nonprotein coding) DNA were run in SYBR green mastermix by qPCR including melting curves as previously detailed [13]. Select genes differentially expressed by microarray (*cMyBP-C*, *MuRF1*, *TNNI3*, *FABP3*, *COL1A*, *PLN*, *NKX2.5*, and β -actin) were analyzed by RT-qPCR as previously detailed [14]. PCR primers and fluorogenic probes [reporter dye, FAM (F); quencher dye, TAMRA (Q)] were created using Primer Express (Table 1) and quantified using the ABI Prism 7700 sequence detector (PE Biosystems, Foster City, CA, USA). GraphPad Prism 6 (GraphPad Prism Software Inc., La Jolla, CA, USA) was used to determine significant statistical difference by one-way analysis of variance followed by post hoc analysis using the Holm–Sidak method. A *P* value < .05 was considered significant.

2.6. Microarray RNA isolation, cDNA amplification/labeling, hybridization, data analysis, and statistics

Total RNA from heart was isolated using the All Prep DNA/RNA/Protein isolation kit (Qiagen, Inc., Valencia, CA, USA) and verified for integrity using the BioAnalyzer 2100 (Agilent Technologies, Inc., Santa Clara, CA, USA). RNA samples labeled with cyanine-5 CTP in a T-7 transcription reaction using the Agilent Low Input Linear RNA Amplification/Labeling System were hybridized to Agilent 4x44K microarray slides (GPL4134 platform, Catalog #G4122F; Agilent Technologies, Inc.) in the presence of equimolar concentrations of cyanine-3 CTP-labeled mouse reference RNA [15]. Slides were hybridized, washed, and scanned on an Axon 4000b microarray scanner, and data were processed using Feature Extraction (version 9.1.3.1; Agilent). Postprocessing included loess-centered [16,17] and median-centered normalization using GeneSpring GX (version 10.0.1 Build 81217; Agilent). The Database for Annotation, Visualization and Integrated Discovery (DAVID)

[16,17] identified significantly enriched functional clusters (high classification stringency, group enrichment score of >1.3 , $P<.05$) using multiple annotation libraries from lists of differentially expressed genes and using the genes represented on the microarray as background (see Supplementary Table 1 for DAVID annotation libraries used). Complete, MIAME-compliant data sets were deposited with the Gene Expression Omnibus of the National Center for Biotechnology Information (<http://www.ncbi.nlm.nih.gov/geo/>) [18] and are accessible through GEO Series accession number GSE68480.

The processing of all sample files — including the generation of images and the conducting of statistical comparisons — was performed using R Programming Language (R). In brief, raw/normalized data were inputted using the “read.maimages” function of the “limma” R package. For statistical comparisons, the study design model was first created (represented as a matrix) by identifying sample groupings based on the following variables: (1) MuRF1 $-/-$ or MuRF1 $+/+$, (2) time point, and (3) fenofibrate-integrated or sham chow diet. Individual comparisons within the study design model were then conducted by first fitting a linear statistical model through each probe across the samples going into each comparison using “lmfit” (limma). The linear fit for each comparison was subsequently modified using the empirical Bayes (“eBayes”) approach, which aims to bring the probe-wise variances across samples to common values, resulting in modified t statistics, F statistic, and log odds differential expression ratios. Finally, for each comparison, log fold change (logFC), P value, and corrected P value (false discovery rate, or FDR) was output. MA plots for each comparison were generated using “plotMA” (limma), plotting average log₂ expression vs. logFC. Gene enrichment using GenBank accessions as keys was performed using the Database for Annotation, Visualization, Integration and Discovery (<http://david.abcc.ncifcrf.gov/>). Where available, each gene was annotated with Gene Ontology (GO; cellular component, biological process, and molecular function databases) and also KEGG and BioCarta pathways. GO enrichment analysis was visualized using R 3.1.0. Hierarchical clustering with the Euclidean metric and complete linkage was performed to group genes based on their log₂ fold change in expression. The heatmap.2() function in the gplots (<http://cran.r-project.org/web/packages/gplots/index.html>) package in R was used to create the heatmaps of the GO fold enrichment scores resulting from the DAVID analysis.

3. Results

The fibric acid derivative fenofibrate is used clinically for the treatment of hypertriglyceridemia and mixed dyslipidemia in patients not responding to nonpharmacological therapies. The lipid-modifying effects of fenofibrate are mediated by its activation of PPAR α in the liver [inhibiting the synthesis and release of very low density lipoproteins and increasing apolipoprotein A-I (apoA-I) and apolipoprotein A-II (apoA-II)] and small intestine (stimulating apoA-I), and an increase in lipoprotein lipase in skeletal muscle [19]. Fenofibrate also has more pleiotropic effects, not related to lipid metabolism including the reduction of fibrinogen, C-reactive protein, and other inflammatory markers that may contribute to its clinical efficacy, particularly microvascular disease [20]. MuRF1 $-/-$ mice were fed a standard mouse chow with 0.05% fenofibrate continuously for 8 weeks and followed by conscious echocardiography for function (Fig. 1A). Heart, liver, and

skeletal muscle samples were harvested at both 3 and 8 weeks for histological analysis, gene expression, and serum chemistry analysis (Fig. 1B).

Like the effects seen clinically in patients with hypercholesterolemia, MuRF1^{-/-} and MuRF1^{+/+} mice achieved improvements in serum triglyceride concentrations by 8 weeks of treatment with fenofibrate (Fig. 1C). Only minor differences between MuRF1^{-/-} and sibling age-matched MuRF1^{+/+} mice were seen over the course of fenofibrate treatment, notably significantly decreased low-density lipoprotein at 8 weeks of treatment (Fig. 1D). Glucose levels were in the reference range throughout the study (<100 mg/dl) and did not differ between MuRF1^{-/-} and MuRF1^{+/+} mice (Fig. 1D).

Histologically, MuRF1^{-/-} hearts did not differ in size in sibling age-matched cardiac sections (Fig. 1E). By gross and histological analysis, no evidence of inflammation was identified (Fig. 1E). No differences in fibrosis were identified by digital image quantification of Masson's trichrome staining for collagen (Fig. 1F). As with previous studies of MuRF1^{-/-} hearts [2,8], no histological evidence of pathology or other differences was identified compared to MuRF1^{+/+} hearts.

We next investigated genes regulated by PPAR α in MuRF1^{-/-} and MuRF1^{+/+} control hearts, skeletal muscle, and the liver (Fig. 2). The PPAR α transcription factor broadly regulates FA and glucose metabolism in mice and humans. In mice, PPAR α activation induces genes coding for the FA transporter CD36 and the FA binding protein 1 (*FABP1*), which are responsible for transporting FAs from the plasma membrane to the nucleus [21,22]. Carnitine palmitoyl transferase 1 (CPT1) encodes for a FA transporter that converts acyl-carnitine to acyl-CoA and is up-regulated transcriptionally by PPAR α agonists [23]. PPAR α also increases PGC-1 expression [24], a protein co-activator of PPAR α [25]. Counteracting these proteins to increase the FA utilization of cells, PPAR α activity also enhances pyruvate dehydrogenase kinase 4 (PDK4) expression. In the present study, we identified that fenofibrate treatment induced expression of cardiac *pdh4* mRNA (Fig. 2A), *cpt-1*, and *pgc-1* mRNA in the gastrocnemius (Fig. 2B) and liver (Fig. 2C). A number of other reported PPAR α genes were also assayed in the heart (Supplementary Fig. 1A), gastrocnemius (Supplementary Fig. 1B), and liver (Supplementary Fig. 1C) in MuRF1^{-/-} and MuRF1^{+/+} mice, including *fatp1*, *Prkaa2* (AMP-activated alpha 2 catalytic subunit), *acox1*, *fabp3*, *fabp4*, and *lpl*. The expression of these genes was not increased in response to fenofibrate treatment, with the exception of *fatp-1* and *lpl* mRNA in the liver (Supplementary Fig. 1C). MuRF1^{-/-} hearts did not exhibit significantly differ from MuRF1^{+/+} with respect to PPAR α -associated genes in sham or 3/8-weeks fenofibrate treatment.

MuRF1 has recently been reported to interact with multiple proteins found in mitochondria [26], with increased cardiac MuRF1 expression affecting mitochondrial ROS production in vivo [27]. Because fenofibrate can affect cardiac mitochondrial respiration [28–30], we next investigated mitochondria number and ultrastructure in MuRF1^{-/-} hearts after fenofibrate treatment (Fig. 3). DNA was isolated MuRF1^{-/-} hearts and quantitatively analyzed for mitochondrial CO1 (aka mt-CO1), Cyt-b (aka mt-Cyb), and ND1 (aka mt-nd1) DNA normalized to nuclear H19 (Imprinted maternally expressed transcript, nonprotein coding) DNA by qPCR (Fig. 3A). The composite of the three genes demonstrates the MuRF1^{-/-}

hearts do not have different DNA number in Chow controls or after 3/8 weeks of fenofibrate treatment (Fig. 3A). Of the three individual mitochondrial C01, Cytb, and ND1 expression assayed, MuRF1 exhibited significant decreases in cardiac C01 at 3 weeks (with trends at 8 weeks of decreased expression) (Supplementary Fig. 2A). Ultrastructurally, chow-treated MuRF1^{-/-} control hearts do not differ from MuRF1^{+/+} sibling controls by transmission electron microscopy, as previously described (data not shown) [2]. After 3 weeks of fenofibrate treatment, no changes in sarcomere ultrastructure were observed (Fig. 3B vs. 3C, for example). Subtle changes were seen in the sub-sarcomemmal mitochondria, including qualitatively more vesicles (Fig. 3C, D). Periodic, disrupted mitochondria were also seen more frequently in MuRF1^{-/-} hearts by TEM (Fig. 3E), suggesting a role of MuRF1 in maintaining mitochondrial integrity upon treatment with fenofibrate. These findings were cardiac specific, as analysis of MuRF1^{-/-} gastrocnemius from the same animals did not reveal any histological differences compared to MuRF1^{+/+} and chow-fed animals (Supplementary Fig. 3). Given MuRF1's role in regulating (inhibiting) ROS production and fenofibrate-regulation of mitochondrial respiration, these findings may indicate MuRF1' integral role in PPAR α -mediated changes in respiration in vivo.

With our recent discovery that MuRF1 inhibits PPAR α activity in vivo, with MuRF1^{-/-} hearts having 500% found in MuRF1^{+/+} controls [9], identifying the effects of fenofibrate on MuRF1^{-/-} cardiac function and structure was a key focus of these studies. Conscious echocardiography was performed on mice at baseline, and 3 weeks and 8 weeks after fenofibrate treatment was given (Fig. 4). As expected, fenofibrate treatment did not affect the hearts of MuRF1^{+/+} mice over the course of the study, including anterior and posterior wall thickness (Fig. 4A). However, MuRF1^{-/-} hearts significantly increased in wall thickness at both 3 and 8 weeks (Fig. 4A). Fenofibrate did not significantly alter MuRF1^{-/-} or MuRF1^{+/+} systolic function, body weight, or heart rate at 3 and 8 weeks (Fig. 4B). MuRF1^{-/-} hearts did have alterations in baseline interventricular distance (left ventricular end-distance in diastole and systole), which are used to calculate left ventricular mass and left ventricular volumes, which was also greater (Fig. 4C). Representative M-mode images demonstrate this increased interventricular diameter (Fig. 4D).

Since MuRF1 has been implicated in the regulation of cardiac hypertrophy [1,2], we next investigated the possibility that the increased wall thickness represented increased cardiomyocyte size. Cross-sectional analysis of MuRF1^{-/-} cardiomyocyte cross-sectional area was performed at multiple heart levels on biological replicates (Fig. 5A). As in previous studies, chow-fed control MuRF1^{-/-} hearts and sibling MuRF1^{+/+} controls did differ in cross-sectional area (Fig. 5A). However, significant increases in cardiomyocyte cross-sectional area were seen at both 3 weeks (Fig. 5B) and 8 weeks (Fig. 5C), consistent with the development of cardiac hypertrophy in response to fenofibrate stimulation. Similarly, actual heart weight to tibia length at the end of 8 weeks of fenofibrate treatment demonstrated significantly increased weights in MuRF1^{-/-} hearts compared to sibling-matched controls (Fig. 5D). Similarly, gastrocnemius mass/TL was significantly increased at 8 weeks of fenofibrate treatment (Supplementary Fig. 4A), while liver weight was unaffected (Supplementary Fig. 4B). To delineate the underlying mechanisms of fenofibrate-induced cardiac hypertrophy, genes up-regulated with pathological, but not physiological, hypertrophy were assayed in MuRF1^{-/-} and MuRF1^{+/+} hearts by RT-

qPCR. *βMHC*, *BNP*, and skeletal muscle α -actin mRNA were significantly higher in MuRF1^{-/-} hearts (Fig. 5E-G). Since MuRF1 has been implicated in inhibiting physiological cardiac hypertrophy in vivo, with spontaneous physiological cardiac hypertrophy occurring in much older MuRF1^{-/-} mice due to enhanced IGF-1 signaling [1], and decreased proteasome function [31], these findings were surprising.

We next sought to identify the underlying mechanisms of the pathological cardiac hypertrophy induced in MuRF1^{-/-} mice in response to fenofibrate. Comparisons of MuRF1^{+/+} and MuRF1^{-/-} hearts from mice fed control (chow) or chow with fenofibrate for 3 weeks or 8 weeks were made using a 44,000-probe microarray. The differential expression of genes normalized to reference cDNA was then identified by comparing MuRF1^{-/-} cardiac mRNA expression to MuRF1^{+/+} mice fed chow or fenofibrate chow for 3 or 8 weeks. Comparison of chow-fed MuRF1^{-/-} cardiac mRNA expression to MuRF1^{+/+} hearts demonstrated few differences, with only 1 gene >2 log fold change higher and 2 genes <-2 log fold change lower, with MuRF1 lowest expression of all the genes, as expected (Supplementary Table 2).

At 8 weeks of fenofibrate/chow diet, MuRF1^{-/-} hearts differentially expressed 144 genes >4 log fold change or <-4 log fold change compared to MuRF1^{+/+} hearts (Fig. 6A; Supplementary Table 3). Of the 144 genes, 108 were decreased and 36 were significantly greater than fourfold MuRF1^{+/+} (Fig. 6A).

TRANSFAC analysis of these 144 differentially genes for common promoter binding sites identified that 54 had promoter binding sites for the sterol regulatory element-binding transcription factor (SREBP1) ($P=.0001$, Bayes Factor 5); 36/14/20 genes had promoter binding sites for E2F-1/E2F1/E2F ($P=.0002$, .004, .005; Bayes Factor 5/4/4); and 11 genes had promoter binding sites for the COUP transcription factor ($P=.0004$, Bayes Factor 4) (Fig. 6B). More than ~3/4 of these 144 genes had decreased expression in MuRF1^{-/-} hearts compared to MuRF1^{+/+} hearts (Fig. 6C, royal blue in heat map). The remaining genes had increased expression (Fig. 6C, teal in heat map). To delineate the biological significance of the MuRF1^{-/-} heart differentially expressed genes at 8 weeks post-fenofibrate treatment, DAVID analysis was performed on the 144 genes and the DAVID enrichment score plotted in shades of red, right (Fig. 6C). The most represented genes were found in extracellular region categories (Fig. 6C, left). The highest DAVID enrichment scores were seen in (i) sarcomere/contractile fibers; (ii) protease inhibitors; and (iii) hemostasis/sarcomere, as detailed in Fig. 7A, B/Supplementary Fig. 6A, and Fig. 7C/Supplementary Fig. 6B, respectively.

Since MuRF1 is a ubiquitin ligase and has primarily been described to regulate the turnover of proteins, including many sarcomere proteins (e.g., troponin I, myosin heavy chain, and cMyBP-C) by posttranslational modification targeting these proteins for proteasome-dependent degradation experimentally, the transcriptional regulation of these targets was unexpected. For example, the MuRF1^{-/-} hearts had significantly increased cardiac myosin binding protein c (*cMyBP-C*), troponin I (*TnnI3*), myosin light chain-2 (*myl-2*), and *myl-3* expression >4 log fold increased (Fig. 7A; Supplementary Table 3). MuRF1^{-/-} hearts also

have increased expression of phospholamban (*PLN*), plakophilin 2 (*PKP2*), and ANP (*NPPA*) mRNA, involved in the performance/contractility of the heart (Fig. 7A).

Discovered initially in 2001, MuRF1 has not been linked to hemostasis or protease inhibitors to our knowledge. However, a series of studies over the past few years have elucidated fenofibrate's pleiotropic activities beyond PPAR α agonism [20,32], including down-regulation of complement and inflammatory responses [32–34] and alterations in proteases [35,36]. These studies may offer some insight in the finding that MuRF1 $^{-/-}$ hearts had significant decreases in genes categorized as protease inhibitors (Fig. 7B) or involved in hemostasis (Fig. 7C). Of the genes represented in the most GO subcategories and with the highest enrichment scores (bright red), MuRF1 $^{-/-}$ heart expressed <-4 log fold change less cystatin A (*CSTA*; aka *STFA1/STFA3*), jininogen 1 (*KNG1*), apolipoprotein H (*APOH*), and serpin peptidase inhibitor (*SerpinA1B*) (Fig. 7B/C). MuRF1 $^{-/-}$ hearts additionally had significantly decreased expression (<-4 log fold change) of apolipoproteins *ApoB*, *ApoA4*, and the *Serpin A3M*, detailed in Supplementary Fig. 6 (Supplementary Table 3).

To begin to validate these findings in the MuRF1 $^{-/-}$ hearts after 8 weeks of fenofibrate treatment, we analyzed MuRF1 $^{-/-}$ hearts after 3 weeks of fenofibrate treatment to identify if these changes were seen early in the process of MuRF1 $^{-/-}$ cardiac hypertrophy. We identified 25 genes with increased expression >4 log fold change and 86 <-4 log fold change vs. MuRF1 $^{+/+}$ challenged with fenofibrate for 3 weeks (Supplementary Fig. 7A and Supplementary Table 4). Of these 111 differentially expressed genes, 45 had promoter binding sites for the SREBP1 ($P<.0001$, Bayes Factor 6); 27/15 genes had promoter binding sites for E2F-1/E2F1/E2F ($P=.0004$ and $.002$, Bayes Factor 4/3); and 2 genes had promoter binding sites for the PPAR:RXR heterodimer sites on PPAR α ($P=.001$, Bayes Factor 3) (Supplementary Fig. 7B). In addition to mirroring the transcription factors related to the differentially expressed genes SREBP1 and E2F1/E2F, most genes found in GO categories were related to the extracellular region (Fig. 6C; Supplementary Fig. 7C). There were also significantly decreased apolipoproteins found in MuRF1 $^{-/-}$ hearts after 3 weeks of fenofibrate (Supplementary Fig. 7D), including *APOH*, *APOA2*, *APOB_35*, *ApoA4_30*, and *FABP*, which were found in the MuRF1 $^{-/-}$ hearts at 8 weeks (Fig. 7B, C). Lastly, MuRF1 $^{-/-}$ hearts after 3-week fenofibrate treatment had significantly decreased genes involved with hemostasis (Supplementary Fig. 7E), as seen at 8 weeks (Fig. 6C), confirming these changes in independent experiments. Confirmation studies of some of the genes where MuRF1 exhibited increased mRNA were performed using RT-qPCR. MuRF1 $^{-/-}$ hearts (confirmed by PCR; Fig. 8A) exhibited significant increases of *Col1A*, *Pln*, and *Nkx2.5*, (Fig. 8B–D). *MyBPC3*, *FABP3*, and *Tnni3* mRNA were not identified as different (Fig. 8E–G).

4. Discussion

Rare variants in the ubiquitin ligase MuRF1 have recently been reported to be a cause of human hypertrophic cardiomyopathy [37], a malignant modifier of hypertrophic cardiomyopathy caused by other mutations [37,38], and a cause of cardiac and skeletal protein aggregate myopathy [39]. Given that loss-of-function MuRF1 mutations are found in human disease causing human hypertrophic cardiomyopathy [37], understanding the

relationship between MuRF1 and hypertrophy is needed. Clinically, fenofibrate is used to treat dyslipidemia and is therapeutically valuable in lowering serum triglycerides in patients [20]. In the present study, we identified an unexpected link between fenofibrate and cardiac hypertrophy in MuRF1^{-/-} hearts at doses that effectively lowered serum triglyceride levels after 8 weeks of treatment (Fig. 1C). The standard dose of fenofibrate used in the present study of 0.05%, which has been estimated to be about 65 mg/body weight/day, equivalent to 1.5 times the recommended human dose on the basis of mg/m² (20 times the human dose based on body weight comparisons) [40]. The spontaneous induction of cardiac hypertrophy in the absence of MuRF1 may be clinically important in patients with known or suspected mutations in MuRF1 and should be considered when treating and monitoring hypertrophic cardiomyopathy patients in the future.

In the present study, the development of MuRF1^{-/-} cardiac hypertrophy in response to fenofibrate represents the induction of pathological cardiac hypertrophy. Characterized by significant increases in anterior and posterior wall thickness (Fig. 4A) and cardiomyocyte cross-sectional area (Fig. 5A–C) in as little as 3 weeks, the activation of β MHC, BNP, and skeletal muscle α -actin in mice with increased heart weight/tibia length (Fig. 5D–G) is diagnostic of pathologic hypertrophy. This should be contrasted with the spontaneous development of physiological hypertrophy in MuRF1^{-/-} mice reported to occur at 9+ months of age by our group [1] and others [41]. Interestingly, both reports identified the enhanced IGF-1/Akt signaling as a mechanism in the absence of pathological hypertrophy markers, such as β MHC, ANP, and BNP mRNA [1,41].

The role of PPAR α activation in cardiomyopathy and hypertrophy has been eluded to in diabetic cardiomyopathy, where excessive PPAR α activation, downstream ROS, and lipotoxicity have been implicated [42,43]. Activation of PPAR α has been linked to the cardiomyocyte hypertrophy induced by leptin in cultured neonatal rat cardiomyocytes [44]. Evidence of MuRF1^{-/-} hearts exhibiting exaggerated PPAR α activity, measured by PPAR α -associated genes compared to MuRF1^{+/+} hearts was limited. Of the PPAR α -regulated genes investigated, MuRF1^{-/-} hearts had a significantly increased *PDK4* mRNA compared to MuRF1^{+/+} hearts after fenofibrate treatment, while gastrocnemius exhibited significant increases in *CD36* (Fig. 2). Increasing expression of *PDK4* in the heart itself has not been reported to be pathologic in vivo [45] and has been shown to trigger an adaptive metabolic response [46]. Alterations in mitochondrial size and lipid accumulation have been associated with increased PPAR α activation [47]. However, no changes in mitochondrial number and only minimal qualitative alterations were identified in MuRF1^{-/-} hearts post-fenofibrate feeding up to 8 weeks (Fig. 3). Together, these observations illustrate only minor contributions of increased PPAR α activity in MuRF1^{-/-} hearts to the induction of pathological activity.

The strongest evidence for the phenotype identified in the present study is MuRF1's transcriptional regulation of SREBP1 and E2F1. Notably in the microarray signature of the MuRF1^{-/-} hearts after 8 weeks of fenofibrate treatment, 54 genes ($P=.0001$, Bayes Factor 5) with SREBP1 promoter binding sites were differentially expressed of the 144 identified (Fig. 6B). It is important to note that SREBP1 and E2F1 activities were not measured directly here, but should be investigated in future studies. In a previous study, we identified

that the lack of both MuRF1 and MuRF2 (MuRF1^{-/-}/MuRF2^{-/-}) altered the regulation of E2F1 activity measured by chromatin IP studies (occupying the promoter of p21, Brip1, PDK4), but did not address how MuRF1 alone regulated E2F1 [48]. Since MuRF1^{-/-} mice have an increased PPAR α activity (REF), another possibility is that PPAR α regulates SREBP1 and E2F1. But the evidence for PPAR α regulation of SREBP-1 and E2F1 is sparse, including the finding that PPAR α ^{-/-} mice have altered SREBP-sensitive gene expression in the liver [49] and in vascular smooth muscle, PPAR α agonists target the E2F/p16/RB transcriptional cascade to repress cell cycle-dependent telomerase activation [50]. Increasing expression of the SREBP-1 transcription factor itself increases cardiomyocyte mass [51]. In skeletal muscle, SREBP-1 regulates muscle protein synthesis, with increasing SREBP-1 enhancing MYOD1, MYOG, and MEF2C factors [52]. In embryonic chick atrial myocytes, SREBP-1 has been described to affect the heart's response to parasympathetic stimulation [53,54].

While fenofibrate activity has been classically attributed to the activation of PPAR α in skeletal muscle and liver [55], this role has not been directly attributed to PPAR α activation in cardiomyocytes. In fact, the concept that fenofibrate has cardioprotective roles independent of its role in lowering cholesterol have been reported by numerous investigators. Clues to these “pleiotropic” effects were reported in the 1980s, with fenofibrate's platelet aggregation reduction reported in 1987 [56]. Later studies found that fenofibrate potentiated warfarin effects [57]. Recent studies of comparative transcriptomic and metabolomics analysis of fenofibrate treatment in mice identified down-regulated genes in blood coagulation and fibrinolysis, overlapping with fish oil treatment [34]. In our studies, the highest differential expressions between any groups were identified between the MuRF1^{-/-} and MuRF1^{+/+} controls (Fig. 6). While significant fenofibrate-induced gene expression changes were observed in MuRF1^{+/+} (Supplementary Table 5) and MuRF1^{-/-} (Supplementary Table 6) hearts after fenofibrate treatment, the degree of change was relatively small. Only 16 genes were >[2] log fold change different in MuRF1^{+/+} hearts at 8-week fenofibrate challenge compared to chow-fed (Supplementary Table 5). MuRF1^{-/-} hearts similarly had only 2 genes >[2] log fold change increased at 8-week fenofibrate challenge compared to chow-fed (Supplementary Table 6). In contrast, 144 genes >[4] log fold change were seen between MuRF1^{-/-} and MuRF1^{+/+} hearts upon challenge with fenofibrate (Fig. 6, Supplementary Table 3). Interestingly, the categories of these genes with the highest expression and enrichment by DAVID analysis were involved in hemostasis and the related protease inhibitor categories in the intact heart (Fig. 6). To our knowledge, these effects by themselves have not been identified at the level of the heart. Here we demonstrate that blocking MuRF1 uniformly inhibits the hemostasis gene expression response in vivo (Fig. 6).

The role of fenofibrate in treating cardiac hypertrophy in diseased states has been confusing, but worth noting given the regulation of MuRF1 in cardiac diseases. Fenofibrate has been reported to ameliorate pressure overload induced cardiac hypertrophy [58–61]. Fenofibrate enhances the association of PPAR α with NFATc4, decreasing its interaction with GATA-4 implicating that PPAR α can compete with GATA-4 binding to NFATc4 to decrease hypertrophy [62]. Suppression of endothelin-1-induced pathological cardiac hypertrophy by fenofibrate has been shown to involve diacylglycerol (DAG) kinase [59,63], GSK3 β [64],

ERK1/2, and cJun kinase [65–67]. Fenofibrate's antihypertrophic response is seen in most studies of pathological hypertrophy, including 2-month-old spontaneously hypertensive rats [68]. But these effects are age-dependent. In contrast, when 6-month-old rats are treated with fenofibrate, paradoxical effects are seen — an aggravation of cardiac hypertrophy [68]. As the present study is the first report of cardiac hypertrophy induction in response to fenofibrate, it potentially links the regulation of PPAR α (by MuRF1) and induction of cardiac hypertrophy by the transcriptional up-regulation SREBP-1 and E2F. While SREBP-1 and E2F activity was not measured directly, their causal relationship with the observed cardiac hypertrophy is one of several possible scenarios that will need to be tested in the future. Moreover, MuRF1's regulation of fenofibrate's pleiotropic non-PPAR α associated genes was unexpected and indicates that inhibition of MuRF1 may be cardioprotective in ways that involve hemostasis in addition to protein quality control and metabolism.

Supplementary Material

Refer to Web version on PubMed Central for supplementary material.

Acknowledgments

The authors wish to thank Vicky Madden (UNC Microscopy Services Laboratory) for her assistance with the preparation and imaging of the transmission electron microscopy, Janice Weaver (University of North Carolina Lineberger Center Animal Histopathology Laboratory) for her consultation and preparation of the histological specimens, Creative Bioinformatics Consultants for assistance with the microarray data analysis, Dr. Hyung-Suk Kim, PhD, and the UNC Animal Clinical Chemistry Laboratory for their assistance with serum chemistry and qPCR analysis.

Funding: This work was supported by the National Institutes of Health (R01HL104129 to M.W.), a Fellowship from the Jefferson-Pilot Corporation (to M.W.), and the Fondation Leducq Transatlantic Networks of Excellence (to M.W.).

Abbreviations

ANP	atrial natriuretic peptide
apoA-I	apolipoprotein A-I
apoA-II	apolipoprotein A-II
APOH	apolipoprotein H
βMHC	beta-myosin heavy chain
MYH7	myosin heavy chain 7
BNP	brain natriuretic peptide
cJun	Jun proto-oncogene
cMyBP-c	cardiac myosin binding protein-c
Col1A	collagen, type I, alpha I
cpt1	carnitine palmitoyltransferase 1A
cTnI	cardiac troponin I

CSTA	cystatin A
DAVID	Database for Annotation, Visualization and Integrated Discovery
E2F-1/E2F1	E2F transcription factor (1)
FA	fatty acid
FABP1	fatty acid binding protein 1
FABP3	fatty acid binding protein 3
FABP4	fatty acid binding protein 4
FATP1	fatty acid transporter, aka SLC27A1 (solute carrier family 27 member 1)
H19	imprinted maternally expressed transcript (nonprotein coding)
KNG1	kininogen 1
IGF-1	insulin-like growth factor-1
lpl	lipoprotein lipase
mt-C01	mitochondrial cytochrome <i>c</i> oxidase subunit 1
mt-Cytb	mitochondrial cytochrome <i>b</i>
mt-ND1	mitochondrial NADH dehydrogenase 1
MuRF1	muscle ring finger-1
Myl-2	myosin light chain-2
Myl-3	myosin light chain-3
NKX2.5	NK2 homeobox 5
PGC-1	peroxisome proliferator-activated receptor gamma, coactivator 1 alpha
PPARα	peroxisome proliferator-activated receptor alpha
PDK4	pyruvate dehydrogenase kinase 4
PLN	phospholamban
PKP2	plakophilin 2
SRF	serum response factor
PRKAA2	protein kinase, AMP-activated alpha2 catalytic subunit
SREBP-1	sterol regulatory element binding transcription factor 1
TnnI3	troponin I
Serpin A1B	serpin peptidase inhibitor

References

1. Wadosky KM, Rodriguez JE, Hite RL, Min JN, Walton BL, Willis MS. Muscle RING finger-1 attenuates IGF-I-dependent cardiomyocyte hypertrophy by inhibiting JNK signaling. *Am J Physiol Endocrinol Metab.* 2014; 306:E723–39. [PubMed: 24425758]

2. Willis MS, Ike C, Li L, Wang DZ, Glass DJ, Patterson C. Muscle ring finger 1, but not muscle ring finger 2, regulates cardiac hypertrophy in vivo. *Circ Res.* 2007; 100:456–9. [PubMed: 17272810]
3. Willis MS, Schisler JC, Li L, Rodriguez JE, Hilliard EG, Charles PC, et al. Cardiac muscle ring finger-1 increases susceptibility to heart failure in vivo. *Circ Res.* 2009; 105:80–8. [PubMed: 19498199]
4. Mearini G, Gedicke C, Schlossarek S, Witt CC, Kramer E, Cao P, et al. Atrogin-1 and MuRF1 regulate cardiac MyBP-C levels via different mechanisms. *Cardiovasc Res.* 2010; 85:357–66. [PubMed: 19850579]
5. Cohen S, Brault JJ, Gygi SP, Glass DJ, Valenzuela DM, Gartner C, et al. During muscle atrophy, thick, but not thin, filament components are degraded by MuRF1-dependent ubiquitylation. *J Cell Biol.* 2009; 185:1083–95. [PubMed: 19506036]
6. Fielitz J, Kim MS, Shelton JM, Latif S, Spencer JA, Glass DJ, et al. Myosin accumulation and striated muscle myopathy result from the loss of muscle RING finger 1 and 3. *J Clin Invest.* 2007; 117:2486–95. [PubMed: 17786241]
7. Kedar V, McDonough H, Arya R, Li HH, Rockman HA, Patterson C. Muscle-specific RING finger 1 is a bona fide ubiquitin ligase that degrades cardiac troponin I. *Proc Natl Acad Sci U S A.* 2004; 101:18135–40. [PubMed: 15601779]
8. Willis MS, Rojas M, Li L, Selzman CH, Tang RH, Stansfield WE, et al. Muscle ring finger 1 mediates cardiac atrophy in vivo. *Am J Physiol Heart Circ Physiol.* 2009; 296:H997–1006. [PubMed: 19168726]
9. Rodriguez JE, Liao JY, He J, Schisler JC, Newgard CB, Drujan D, et al. The ubiquitin ligase MuRF1 regulates PPARalpha activity in the heart by enhancing nuclear export via monoubiquitination. *Mol Cell Endocrinol.* 2015; 413:36–48. [PubMed: 26116825]
10. Burkart EM, Sambandam N, Han X, Gross RW, Courtois M, Gierasch CM, et al. Nuclear receptors PPARbeta/delta and PPARalpha direct distinct metabolic regulatory programs in the mouse heart. *J Clin Invest.* 2007; 117:3930–9. [PubMed: 18037994]
11. Oakley RH, Ren R, Cruz-Topete D, Bird GS, Myers PH, Boyle MC, et al. Essential role of stress hormone signaling in cardiomyocytes for the prevention of heart disease. *Proc Natl Acad Sci U S A.* 2013; 110:17035–40. [PubMed: 24082121]
12. Willis MS, Dyer LA, Ren R, Lockyer P, Moreno-Miralles I, Schisler JC, et al. BMPER regulates cardiomyocyte size and vessel density in vivo. *Cardiovasc Pathol.* 2013; 22:228–40. [PubMed: 23200275]
13. Hayashi M, Imanaka-Yoshida K, Yoshida T, Wood M, Fearn C, Tatake RJ, et al. A crucial role of mitochondrial Hsp40 in preventing dilated cardiomyopathy. *Nat Med.* 2006; 12:128–32. [PubMed: 16327803]
14. Kim HS, Lee G, John SW, Maeda N, Smithies O. Molecular phenotyping for analyzing subtle genetic effects in mice: application to an angiotensinogen gene titration. *Proc Natl Acad Sci U S A.* 2002; 99:4602–7. [PubMed: 11904385]
15. He XR, Zhang C, Patterson C. Universal mouse reference RNA derived from neonatal mice. *Biotechniques.* 2004; 37:464–8. [PubMed: 15470901]
16. Riva A, Carpentier AS, Torresani B, Henaut A. Comments on selected fundamental aspects of microarray analysis. *Comput Biol Chem.* 2005; 29:319–36. [PubMed: 16219488]
17. Smyth GK, Speed T. Normalization of cDNA microarray data. *Methods.* 2003; 31:265–73. [PubMed: 14597310]
18. Brazma A, Hingamp P, Quackenbush J, Sherlock G, Spellman P, Stoeckert C, et al. Minimum information about a microarray experiment (MIAME) – toward standards for microarray data. *Nat Genet.* 2001; 29:365–71. [PubMed: 11726920]
19. Knopp RH. Drug treatment of lipid disorders. *N Engl J Med.* 1999; 341:498–511. [PubMed: 10441607]
20. McKeage K, Keating GM. Fenofibrate: a review of its use in dyslipidaemia. *Drugs.* 2011; 71:1917–46. [PubMed: 21942979]
21. Poirier H, Niot I, Monnot MC, Braissant O, Meunier-Durmort C, Costet P, et al. Differential involvement of peroxisome-proliferator-activated receptors alpha and delta in fibrate and fatty-

- acid-mediated inductions of the gene encoding liver fatty-acid-binding protein in the liver and the small intestine. *Biochem J.* 2001; 355:481–8. [PubMed: 11284737]
22. Motojima K, Passilly P, Peters JM, Gonzalez FJ, Latruffe N. Expression of putative fatty acid transporter genes are regulated by peroxisome proliferator-activated receptor alpha and gamma activators in a tissue- and inducer-specific manner. *J Biol Chem.* 1998; 273:16710–4. [PubMed: 9642225]
 23. Aoyama T, Peters JM, Iritani N, Nakajima T, Furihata K, Hashimoto T, et al. Altered constitutive expression of fatty acid-metabolizing enzymes in mice lacking the peroxisome proliferator-activated receptor alpha (PPARalpha). *J Biol Chem.* 1998; 273:5678–84. [PubMed: 9488698]
 24. Chung HW, Lim JH, Kim MY, Shin SJ, Chung S, Choi BS, et al. High-fat diet-induced renal cell apoptosis and oxidative stress in spontaneously hypertensive rat are ameliorated by fenofibrate through the PPARalpha–FoxO3a–PGC-1alpha pathway. *Nephrol Dial Transplant.* 2012; 27:2213–25. [PubMed: 22076434]
 25. Rowe GC, Jiang A, Arany Z. PGC-1 coactivators in cardiac development and disease. *Circ Res.* 2010; 107:825–38. [PubMed: 20884884]
 26. Witt SH, Granzier H, Witt CC, Labeit S. MURF-1 and MURF-2 target a specific subset of myofibrillar proteins redundantly: towards understanding MURF-dependent muscle ubiquitination. *J Mol Biol.* 2005; 350:713–22. [PubMed: 15967462]
 27. Mattox TA, Young ME, Rubel CE, Spaniel C, Rodriguez JE, Grevenko TJ, et al. MuRF1 activity is present in cardiac mitochondria and regulates reactive oxygen species production in vivo. *J Bioenerg Biomembr.* 2014; 46:173. [PubMed: 24733503]
 28. Zungu M, Felix R, Essop MF. Wy-14,643 and fenofibrate inhibit mitochondrial respiration in isolated rat cardiac mitochondria. *Mitochondrion.* 2006; 6:315–22. [PubMed: 17046337]
 29. King KL, Young ME, Kerner J, Huang H, O'Shea KM, Alexson SE, et al. Diabetes or peroxisome proliferator-activated receptor alpha agonist increases mitochondrial thioesterase I activity in heart. *J Lipid Res.* 2007; 48:1511–7. [PubMed: 17438340]
 30. Yao CX, Li WY, Zhang SF, Zhang HF, Zang MX. Effects of doxorubicin and fenofibrate on the activities of NADH oxidase and citrate synthase in mice. *Basic Clin Pharmacol Toxicol.* 2011; 109:452–6. [PubMed: 21711451]
 31. Hwee DT, Gomes AV, Bodine SC. Cardiac proteasome activity in muscle ring finger-1 null mice at rest and following synthetic glucocorticoid treatment. *Am J Physiol Endocrinol Metab.* 2011; 301:E967–77. [PubMed: 21828340]
 32. Okopien B, Krysiak R, Herman ZS. Effects of short-term fenofibrate treatment on circulating markers of inflammation and hemostasis in patients with impaired glucose tolerance. *J Clin Endocrinol Metab.* 2006; 91:1770–8. [PubMed: 16492702]
 33. Lee JJ, Jin YR, Yu JY, Munkhtsetseg T, Park ES, Lim Y, et al. Antithrombotic and antiplatelet activities of fenofibrate, a lipid-lowering drug. *Atherosclerosis.* 2009; 206:375–82. [PubMed: 19345949]
 34. Lu Y, Boekschoten MV, Wopereis S, Muller M, Kersten S. Comparative transcriptomic and metabolomic analysis of fenofibrate and fish oil treatments in mice. *Physiol Genomics.* 2011; 43:1307–18. [PubMed: 21954454]
 35. Khera AV, Qamar A, Reilly MP, Dunbar RL, Rader DJ. Effects of niacin, statin, and fenofibrate on circulating proprotein convertase subtilisin/kexin type 9 levels in patients with dyslipidemia. *Am J Cardiol.* 2015; 115:178–82. [PubMed: 25432415]
 36. Noguchi T, Kobayashi J, Yagi K, Nohara A, Yamaaki N, Sugihara M, et al. Comparison of effects of bezafibrate and fenofibrate on circulating proprotein convertase subtilisin/kexin type 9 and adipocytokine levels in dyslipidemic subjects with impaired glucose tolerance or type 2 diabetes mellitus: results from a crossover study. *Atherosclerosis.* 2011; 217:165–70. [PubMed: 21411093]
 37. Chen SN, Czernuszewicz G, Tan Y, Lombardi R, Jin J, Willerson JT, et al. Human molecular genetic and functional studies identify TRIM63, encoding Muscle RING Finger Protein 1, as a novel gene for human hypertrophic cardiomyopathy. *Circ Res.* 2012; 111:907–19. [PubMed: 22821932]

38. Su M, Wang J, Kang L, Wang Y, Zou Y, Feng X, et al. Rare variants in genes encoding MuRF1 and MuRF2 are modifiers of hypertrophic cardiomyopathy. *Int J Mol Sci.* 2014; 15:9302–13. [PubMed: 24865491]
39. Olive M, Abdul-Hussein S, Oldfors A, Gonzalez-Costello J, van der Ven PF, Furst DO, et al. New cardiac and skeletal protein aggregate myopathy associated with combined MuRF1 and MuRF3 mutations. *Hum Mol Genet.* 2015; 24:3638–50. [PubMed: 25801283]
40. Kuno T, Hata K, Takamatsu M, Hara A, Hirose Y, Takahashi S, et al. The peroxisome proliferator-activated receptor (PPAR) alpha agonist fenofibrate suppresses chemically induced lung alveolar proliferative lesions in male obese hyperlipidemic mice. *Int J Mol Sci.* 2014; 15:9160–72. [PubMed: 24857924]
41. Spangenburg EE, Le Roith D, Ward CW, Bodine SC. A functional insulin-like growth factor receptor is not necessary for load-induced skeletal muscle hypertrophy. *J Physiol.* 2008; 586:283–91. [PubMed: 17974583]
42. Sugden MC, Warlow MP, Holness MJ. The involvement of PPARs in the causes, consequences and mechanisms for correction of cardiac lipotoxicity and oxidative stress. *Curr Mol Pharmacol.* 2012; 5:224–40. [PubMed: 22122452]
43. Kiec-Wilk B, Dembinska-Kiec A, Olszanecka A, Bodzioch M, Kawecka-Jaszcz K. The selected pathophysiological aspects of PPARs activation. *J Physiol Pharmacol.* 2005; 56:149–62. [PubMed: 15985699]
44. Hou N, Luo MS, Liu SM, Zhang HN, Xiao Q, Sun P. Leptin induces hypertrophy through activating the peroxisome proliferator-activated receptor alpha pathway in cultured neonatal rat cardiomyocytes. *Clin Exp Pharmacol Physiol.* 2010; 37:1087–95. [PubMed: 20738325]
45. Zhao G, Jeoung NH, Burgess SC, Rosaen-Stowe KA, Inagaki T, Latif S, et al. Overexpression of pyruvate dehydrogenase kinase 4 in heart perturbs metabolism and exacerbates calcineurin-induced cardiomyopathy. *Am J Physiol Heart Circ Physiol.* 2008; 294:H936–43. [PubMed: 18083902]
46. Chambers KT, Leone TC, Sambandam N, Kovacs A, Wagg CS, Lopaschuk GD, et al. Chronic inhibition of pyruvate dehydrogenase in heart triggers an adaptive metabolic response. *J Biol Chem.* 2011; 286:11155–62. [PubMed: 21321124]
47. Elezaby A, Sverdllov AL, Tu VH, Soni K, Luptak I, Qin F, et al. Mitochondrial remodeling in mice with cardiomyocyte-specific lipid overload. *J Mol Cell Cardiol.* 2015; 79:275–83. [PubMed: 25497302]
48. Willis MS, Wadosky KM, Rodriguez JE, Schisler JC, Lockyer P, Hilliard EG, et al. Muscle ring finger 1 and muscle ring finger 2 are necessary but functionally redundant during developmental cardiac growth and regulate E2F1-mediated gene expression in vivo. *Cell Biochem Funct.* 2014; 32:39–50. [PubMed: 23512667]
49. Patel DD, Knight BL, Wiggins D, Humphreys SM, Gibbons GF. Disturbances in the normal regulation of SREBP-sensitive genes in PPAR alpha-deficient mice. *J Lipid Res.* 2001; 42:328–37. [PubMed: 11254743]
50. Gizard F, Nomiya T, Zhao Y, Findeisen HM, Heywood EB, Jones KL, et al. The PPARalpha/p16INK4a pathway inhibits vascular smooth muscle cell proliferation by repressing cell cycle-dependent telomerase activation. *Circ Res.* 2008; 103:1155–63. [PubMed: 18818403]
51. Lecomte V, Meugnier E, Euthine V, Durand C, Freyssen D, Nemoz G, et al. A new role for sterol regulatory element binding protein 1 transcription factors in the regulation of muscle mass and muscle cell differentiation. *Mol Cell Biol.* 2010; 30:1182–98. [PubMed: 20028734]
52. Dessalle K, Euthine V, Chanon S, Delarichaudy J, Fujii I, Rome S, et al. SREBP-1 transcription factors regulate skeletal muscle cell size by controlling protein synthesis through myogenic regulatory factors. *PLoS One.* 2012; 7:e50878. [PubMed: 23226416]
53. Park HJ, Zhang Y, Du C, Welzig CM, Madias C, Aronovitz MJ, et al. Role of SREBP-1 in the development of parasympathetic dysfunction in the hearts of type 1 diabetic Akita mice. *Circ Res.* 2009; 105:287–94. [PubMed: 19423844]
54. Park HJ, Georgescu SP, Du C, Madias C, Aronovitz MJ, Welzig CM, et al. Parasympathetic response in chick myocytes and mouse heart is controlled by SREBP. *J Clin Invest.* 2008; 118:259–71. [PubMed: 18060044]

55. Balakumar P, Rohilla A, Mahadevan N. Pleiotropic actions of fenofibrate on the heart. *Pharmacol Res.* 2011; 63:8–12. [PubMed: 21093591]
56. Kloer HU. Structure and biochemical effects of fenofibrate. *Am J Med.* 1987; 83:3–8. [PubMed: 3318451]
57. Kim KY, Mancano MA. Fenofibrate potentiates warfarin effects. *Ann Pharmacother.* 2003; 37:212–5. [PubMed: 12549950]
58. Zou J, Le K, Xu S, Chen J, Liu Z, Chao X, et al. Fenofibrate ameliorates cardiac hypertrophy by activation of peroxisome proliferator-activated receptor- α partly via preventing p65-NF κ B binding to NFATc4. *Mol Cell Endocrinol.* 2013; 370:103–12. [PubMed: 23518069]
59. Chen HJ, Chen JZ, Wang XX, Yu M. PPAR α activator fenofibrate regressed left ventricular hypertrophy and increased myocardium PPAR α expression in spontaneously hypertensive rats. *Zhejiang Da Xue Xue Bao Yi Xue Ban.* 2007; 36:470–6. [PubMed: 17924466]
60. Lebrasseur NK, Duhaney TA, DeSilva DS, Cui L, Ip PC, Joseph L, et al. Effects of fenofibrate on cardiac remodeling in aldosterone-induced hypertension. *Hypertension.* 2007; 50:489–96. [PubMed: 17606858]
61. Liang F, Wang F, Zhang S, Gardner DG. Peroxisome proliferator activated receptor (PPAR) α agonists inhibit hypertrophy of neonatal rat cardiomyocytes. *Endocrinology.* 2003; 144:4187–94. [PubMed: 12933694]
62. Le K, Li R, Xu S, Wu X, Huang H, Bao Y, et al. PPAR α activation inhibits endothelin-1-induced cardiomyocyte hypertrophy by prevention of NFATc4 binding to GATA-4. *Arch Biochem Biophys.* 2012; 518:71–8. [PubMed: 22198280]
63. Huang Y, Zhang H, Shao Z, O'Hara KA, Kopilas MA, Yu L, et al. Suppression of endothelin-1-induced cardiac myocyte hypertrophy by PPAR agonists: role of diacylglycerol kinase ζ . *Cardiovasc Res.* 2011; 90:267–75. [PubMed: 21183507]
64. Li R, Zheng W, Pi R, Gao J, Zhang H, Wang P, et al. Activation of peroxisome proliferator-activated receptor- α prevents glycogen synthase 3 β phosphorylation and inhibits cardiac hypertrophy. *FEBS Lett.* 2007; 581:3311–6. [PubMed: 17597616]
65. De Silva DS, Wilson RM, Hutchinson C, Ip PC, Garcia AG, Lancel S, et al. Fenofibrate inhibits aldosterone-induced apoptosis in adult rat ventricular myocytes via stressactivated kinase-dependent mechanisms. *Am J Physiol Heart Circ Physiol.* 2009; 296:H1983–93. [PubMed: 19395558]
66. Li CB, Li XX, Chen YG, Zhang C, Zhang MX, Zhao XQ, et al. Effects and mechanisms of PPAR α activator fenofibrate on myocardial remodelling in hypertension. *J Cell Mol Med.* 2009; 13:4444–52. [PubMed: 18754816]
67. Irukayama-Tomobe Y, Miyauchi T, Sakai S, Kasuya Y, Ogata T, Takanashi M, et al. Endothelin-1-induced cardiac hypertrophy is inhibited by activation of peroxisome proliferator-activated receptor- α partly via blockade of c-Jun NH2-terminal kinase pathway. *Circulation.* 2004; 109:904–10. [PubMed: 14967736]
68. Purushothaman S, Sathik MM, Nair RR. Reactivation of peroxisome proliferator-activated receptor α in spontaneously hypertensive rat: age-associated paradoxical effect on the heart. *J Cardiovasc Pharmacol.* 2011; 58:254–62. [PubMed: 21654328]

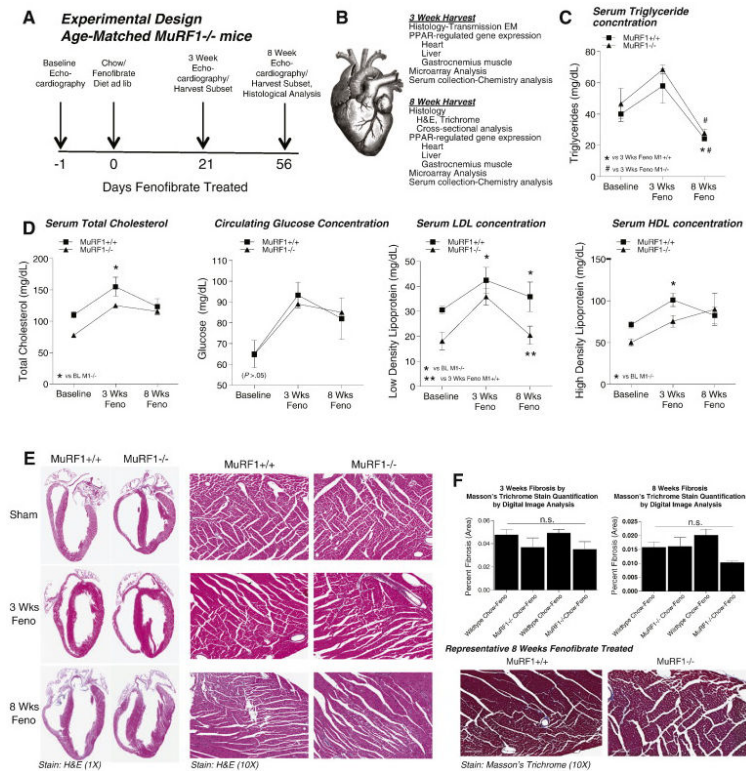
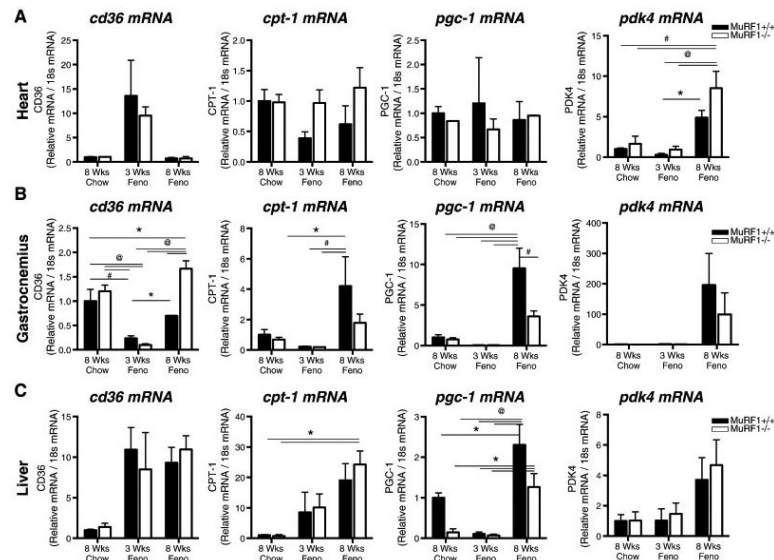


Fig. 1. MuRF1^{-/-} hearts challenged with the PPAR α agonist fenofibrate. (A) Experimental design. (B) Individual studies performed. (C) Fasting serum triglyceride levels. (D) Fasting total cholesterol, glucose concentration, LDL, and HDL. (E) Histological analysis of H&E-stained hearts. (F) Fibrosis analysis of Masson's trichrome-stained hearts. $n=7$, 4 , and 6 mice for baseline, 3-week, and 8-week time points, respectively. Data are mean \pm S.E.M. A one-way analysis of variance was used to determine significance. * $P<.05$ vs. baseline (BL) MuRF1^{-/-}. ** $P<.05$ vs. 3-week fenofibrate fed MuRF1^{+/+}; # $P<.05$ vs. 3 Weeks of fenofibrate fed MuRF1^{-/-}.

**Fig. 2.**

Quantitative analysis of PPAR-regulated genes from MuRF1^{-/-} mice. RT-qPCR analysis of *cd36*, *cpt-1*, *pgc-1*, and *pdk4* from (A) hearts, (B) skeletal muscle, and (C) liver from control chow-fed mice (8-week chow), and 3- and 8-week postfenofibrate/chow treatment. $n=4$ mice/group. Data are mean \pm S.E.M. A one-way analysis of variance was used to determine significance. * $P<.05$; # $P<.01$; @ $P<.001$.

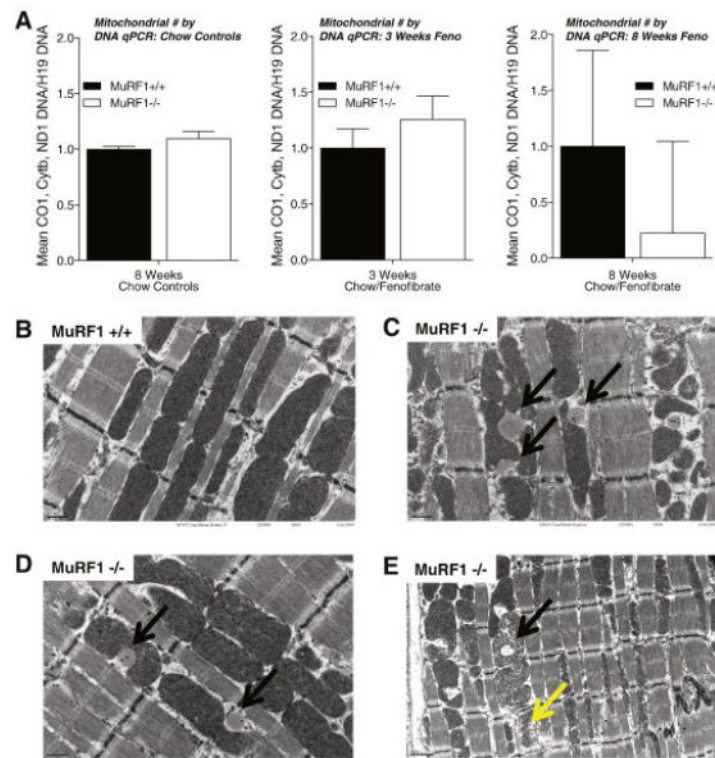
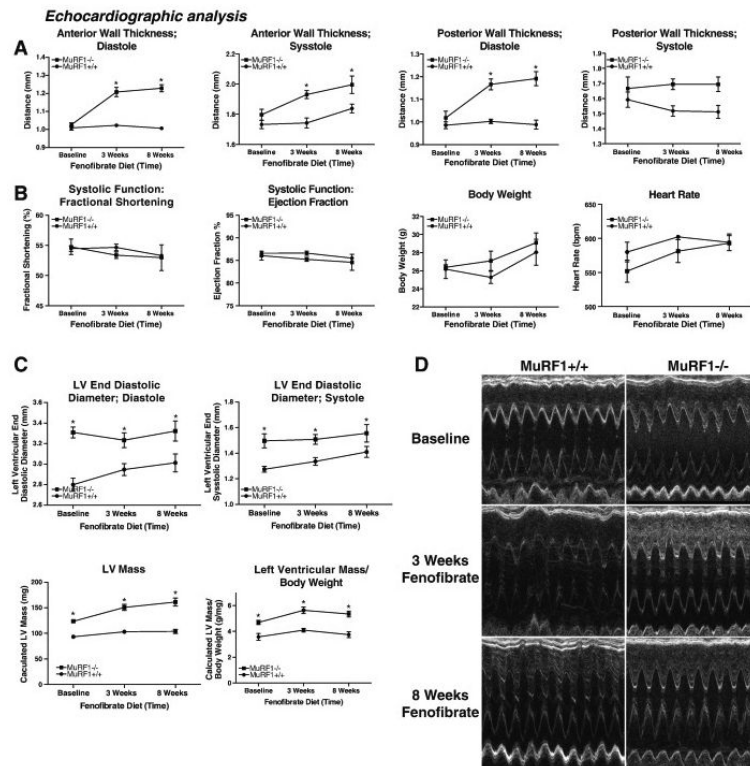
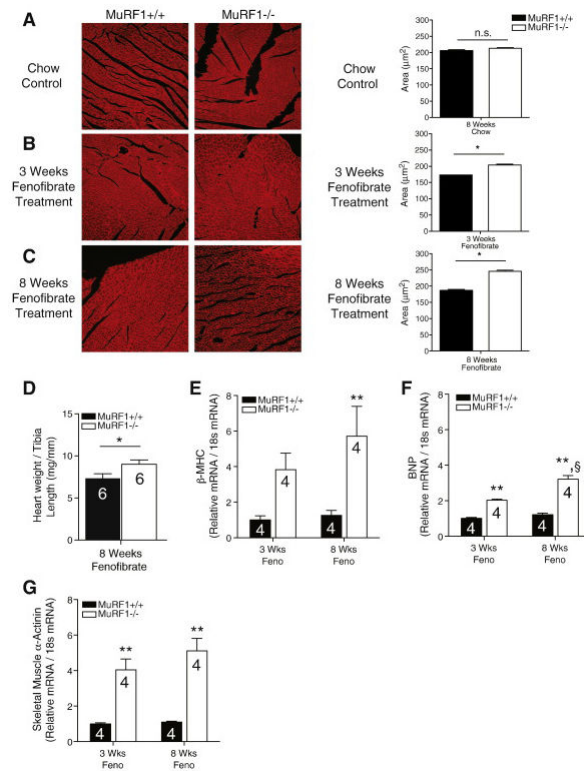


Fig. 3.

Quantitative and ultrastructural analysis of MuRF1^{-/-} mitochondria after fenofibrate challenge. (A) Quantitative analysis of the mean cytochrome *c* oxidase subunit 1 (CO1; aka mt-CO1)/cytochrome *b* (Cyt-b; aka mt-Cyb)/NADH dehydrogenase 1 (ND1; aka mt-nd1) normalized to nuclear H19 (Imprinted maternally expressed transcript, nonprotein coding) in chow-fed control mice (left) and after 3 weeks (middle) and 8-week fenofibrate treatment (right) via fenofibrate/chow (0.05% wt/wt). Expression of individual mt-CO1, mt-Cyb, and mt-ND1 is detailed in Supplementary Fig. 2. (B–E) Transmission electron microscopy analysis of MuRF1^{-/-} hearts reveal ultrastructural changes not seen in MuRF1^{+/+} after 3-week fenofibrate feeding. An increase in vesicles found around and in the mitochondria were identified in MuRF1^{-/-} hearts (black arrows), as were mitochondrial disruption (yellow arrow). The vesicles were not found in wild-type mice (lower right) or in chow-fed age-matched MuRF1^{-/-} mice. (B–D) 20,000 \times ; (E) 10,000 \times , scale in lower left corner of each image. $n=4$ mice/group. Data are mean \pm S.E.M. A Student's *t* test was used to determine significance; $P<.05$ was considered statistically significant.

**Fig. 4.**

Echocardiographic analysis of MuRF1^{-/-} hearts with fenofibrate challenge in vivo. Serial echocardiographic analysis of conscious mice (~50% male/50% female) at baseline, 3-week, and 8-week fenofibrate treatment. (A) Anterior and posterior wall thickness in systole and diastole. (B) Systolic function $FS\% = [(LVEDD - LVESD) / LVEDD] \times 100$; $EF\% = [(LV\ Vol;d - LV\ Vol;s) / LV\ Vol;d] \times 100$, body weight, and heart rates. (C) Left ventricular (LV) end-distance in diastole (LVEDD) and systole (LVESD) used to calculate the LV mass = $[1.055 \times (ExLVD; d^3 - LVEDD; d^3)]$ and LV volumes $[LV\ volume\ in\ diastole\ (LV\ Vol;D) = (7/2.4 + LVEDD) \times LVEDD^3 \times 1000, LV\ Vol;S = (7/2.4 + LVESD) \times LVESD^3 \times 1000]$. (D) Representative m-mode echos of MuRF1^{-/-} and sibling MuRF1^{+/+} hearts at baseline and 3/8-week postfenofibrate treatment. $n=9, 6,$ and 13 MuRF1^{+/+} mice (at baseline, 3-, and 8-week fenofibrate, respectively) and $n=12, 6,$ and 7 MuRF1^{-/-} mice (at baseline, 3-, and 8-week fenofibrate, respectively). Data are mean \pm S.E.M. A one-way analysis of variance was used to determine significance and compared to MuRF1^{+/+} baseline. $*P < .05$ vs. baseline MuRF1^{+/+}.

**Fig. 5.**

Morphometric and molecular analysis of cardiac hypertrophy in MuRF1^{-/-} mice post-fenofibrate treatment. (A) Chow control, (B) 3-week, and (C) 8-week postfenofibrate treatment. (D) Measured heart weight/tibia length. (E) RT-qPCR analysis of β-MHC. (F) BNP. (G) Skeletal muscle α-actinin mRNA after 3- and 8-week fenofibrate treatment. Data are mean±S.E.M. (A–C) *n*=400 cardiomyocytes from 2 mice/group. (A–C) Student's *t* test was used to determine significance. **P*<.05 vs. MuRF1^{+/+}. D: *n*=6 mice/group. A Student's *t* test was used to determine significance. **P*<.05 vs. MuRF1^{+/+}. (E–G) *n*=4 mice/group. A one-way analysis of variance was used to determine significance, ***P*<.05 vs. 3-week fenofibrate-fed MuRF1^{+/+}, §*P*<.05 vs. 3-week fenofibrate-fed MuRF1^{-/-}.

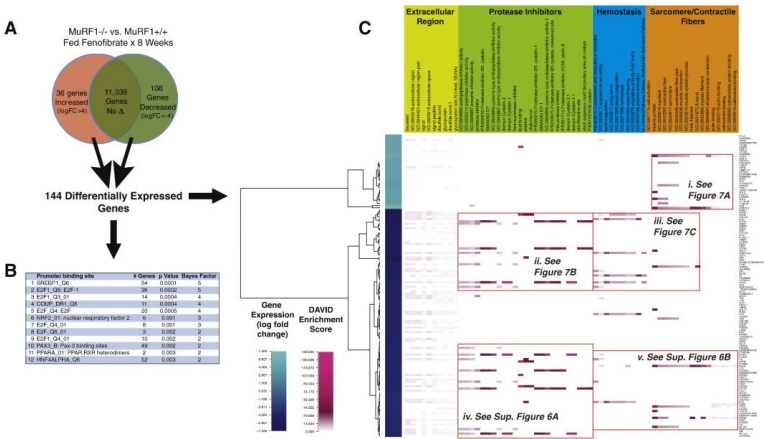
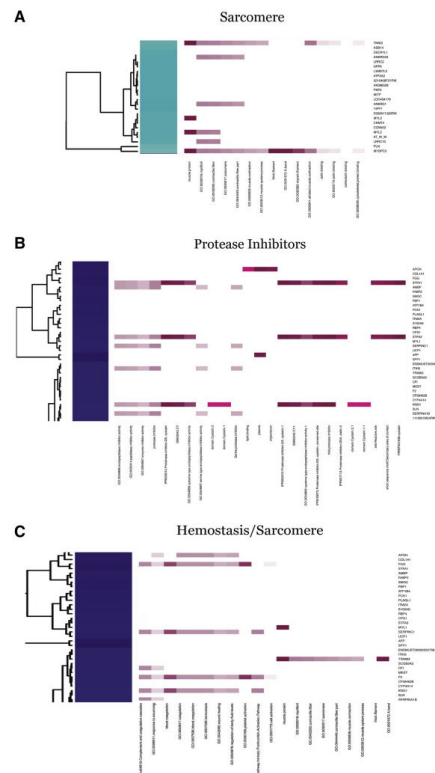
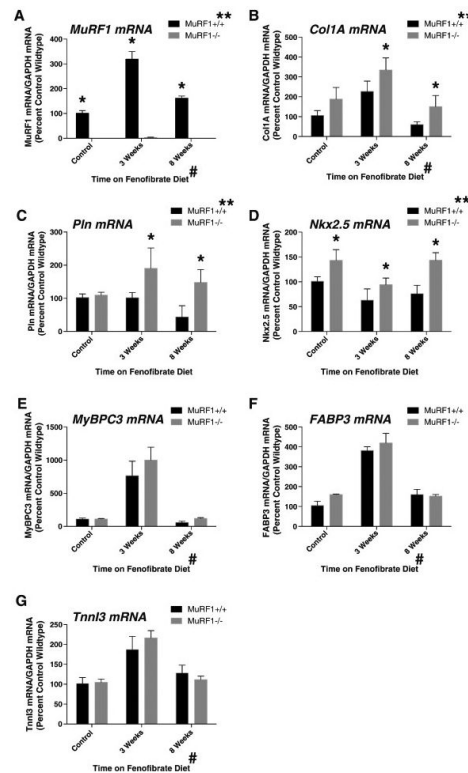


Fig. 6. Hypercluster analysis of MuRF1^{-/-} mRNA by microarray at 8-week fenofibrate treatment compared to sibling MuRF1^{+/+} hearts. (A) Differentially expressed genes reaching significance and >4 or <-4 log fold change compared to MuRF1^{+/+} (=1) were identified for further bioinformatics analysis. (B) TRANSFAC analysis of these 144 genes was performed for common promoter binding sites and statistically analyzed for significance and given a Bayes Factor. (C) Graphical representation of the 144 genes differentially expressed and their analysis by DAVID for Gene Ontology categories reaching increased enrichment (as indicated by figure legend). Subcategories outlined in red are detailed in Fig. 7 and Supplementary Fig. 6, as indicated in the inserts. Raw data used for analysis can be found in Supplementary Table 2. *n*=3/group.

**Fig. 7.**

Gene detail of the MuRF1^{-/-} heart hypercluster subgroups of the most highly enriched Gene Ontology categories 8 weeks after fenofibrate treatment using DAVID. The Database for Annotation, Visualization and Integrated Discovery (DAVID) [16,17] categories with the highest enrichment scores include those broadly falling into the (A) sarcomere, (B) protease inhibitors, and (C) hemostasis/sarcomere, enlarged from Fig. 6C, top 3 boxes.

**Fig. 8.**

Quantitative analysis of mRNA from MuRF1^{-/-} hearts used in the microarray analysis. RT-qPCR analysis of (A) muscle ring finger-1 (MuRF1) mRNA; (B) collagen, type i, $\alpha 1$ (Col1A) mRNA; (C) phospholamban (Pln) mRNA; (D) NK2 homeobox 5 (Nkx2.5) mRNA; (E) myosin binding protein C (MyBPC3) mRNA; (F) fatty acid binding protein 3, muscle and heart (FABP3) mRNA; and (G) troponin i type 3 (Cardiac) (TnnI3) mRNA normalized to GAPDH. Control and 8 weeks of fenofibrate treatment, $n=3$ /group; 3 weeks of fenofibrate treatment, $n=4$ /group. Data are mean \pm S.E.M. A two-way analysis of variance followed by post hoc multiwise comparison was used to determine significance. # $P < .05$ fenofibrate vs. chow control. ** $P < .05$ MuRF1^{-/-} vs. sibling-matched MuRF1^{+/+}; * $P < .05$.

Table 1

Primers and probe sets used in FAM-based RT-qPCR analysis of cardiac mRNA

Myosin binding protein (MyBPC3)	
Forward:	CAG TGC AGG AGA TAC TGC AA
Reverse:	CTT TCT TCT GGA TGG TCT GG
Probe:	FAC CAC GGC TCC AAC TGC CCA GAC AQ
MuRF1 (Trim63)	
Forward:	TCC TGC AGA GTG ACC AAG GA
Reverse:	ATG GCG TAG AGG GTG TCA AA
Probe:	FTG ACT CAG CTC CTC CTT CAC CTG GQ
Troponin I (TnnI3)	
Forward:	CAG GTG AAG AAG GAG GAC AT
Reverse:	GCC ACT CAG TGC ATC GAT AT
Probe:	FTG CGC CAG TCT CCC ACC TCC CGQ
Fatty acid binding protein 3 (Fabp3)	
Forward:	AAC TAG GGA GCT AGT TGA CG
Reverse:	CTT CTC ATA AGT CCG AGT GC
Probe:	FAC CAC ACT GCC ATG AGT GAG AGT CAG Q
Collagen 1A (Col1A)	
Forward:	AGA GCA TGA CCG ATG GAT TC
Reverse:	ATT AGG CGC AGG AAG GTC AG
Probe:	FCT CCG ACC CCG CCG ATG TCG Q
Phospholamban (Pln)	
Forward:	GCT GCT GAT CTG CAT CAT TGT
Reverse:	TGC TCG GCT TTA AGC TGA GT
Probe:	FAG CTG CCG CCA CTC CAG ACC TGC AQ
Nkx2.5	
Forward:	ACC CTG ACC CAG CCA AAG A
Reverse:	GGC TTT GTC CAG CTC CAC T
Probe:	FAG AGC TGT GCG CGC TGC AGA AGQ
GAPDH	
Forward:	AGG TCG GTG TGA CCG GAT TT
Reverse:	GGC AAC AAT CTC CAC TTT GC
Probe:	FTG CAA ATG GCA GCC CTG GTG ACC AQ

Sequences created using Primer Express, as detailed in Materials and Methods. All reactions were run with the F; 5'-Fluorescein (FAM) and the Q (indicated below) Quencher (TAMRA) as previously described by Kim et al. [14].